Self-Correction of 3D Reconstruction from Multi-view Stereo Images

Xiangyang Ju
School of Computing
The Robert Gordon University
Aberdeen AB25 1HG, UK
x.ju@rgu.ac.uk

J Paul Siebert
Department of Computing Science
Glasgow University
Glasgow G12 8QQ, UK
psiebert@dcs.gla.ac.uk

Balvinder S Khambay
Glasgow Dental Hospital and School
Glasgow G2 3JZ , UK

Ashraf F Ayoub
Glasgow Dental Hospital and School
Glasgow G2 3JZ , UK

Abstract

We present a self-correction approach to improving the 3D reconstruction of a multi-view 3D photogrammetry system. The self-correction approach has been able to repair the reconstructed 3D surface damaged by depth discontinuities. Due to self-occlusion, multi-view range images have to be acquired and integrated into a watertight non-redundant mesh model in order to cover the extended surface of an imaged object. The integrated surface often suffers from "dent" artifacts produced by depth discontinuities in the multi-view range images. In this paper we propose a novel approach to correcting the 3D integrated surface such that the dent artifacts can be repaired automatically. We show examples of 3D reconstruction to demonstrate the improvement that can be achieved by the self-correction approach. This self-correction approach can be extended to integrate range images obtained from alternative range capture devices.

1. Introduction

In this paper we introduce a self-correction approach to improving the reconstruction of 3D shape from multi-view stereo images which automatically repairs damaged 3D surfaces integrated from multi-view range images.

Self-occlusion is always a source of deficiency in 3D shape reconstruction, either by laser scanning or stereo photogrammtry. Due to self-occlusion, a single stereo-pair of images can only serve to reconstruct a range image that represents a partial surface of an object. Several range images from different view angles are inevitably required to recover the complete view-space of the object surface. The range images acquired by means of multi-view stereo photogrammetry need to be registered and integrated. Here we assure that the transformations between pairs of range images are reliably estimated by calibration [14, 29, 34, 38, 39]. We focus on range image integration issues in our multi-view 3D photogrammetry system [13].

Multi-view range image integration can be categorized into four major approaches: point based methods [4, 10, 18, 23, 37, 40], direct surface merging [12, 15, 26, 31, 33, 35, 36, 41], volumetric approaches employing implicit surfaces [1, 2, 7, 8, 9, 21, 22, 25, 27, 28] and model based methods [24, 32]. Volumetric diffusion [3] and volumetric graph-cuts [30] have been proposed to build watertight 3D models from multi-views and especially focus on filling holes in the models. Dyer [5] presented a review of reconstruction methods based on multiple views. There are also approaches [15, 16, 17, 24, 32] which combine range images and 2-D silhouette information [11] to assist the integration process.

Point based methods [4, 10, 18, 23, 37, 40] have the merit of constructing surfaces from points directly and efficiently, but surfaces integrated from range data points tend to be of poor quality due to range data noise and registration errors. Soucy and Laurendeau [31] pointed out that computing a surface model from only range data points would lead to a model having the accuracy of the worst measured data point. The point based methods may fail if sample noise approaches sample density. In direct surface merging approaches [12, 15, 26, 31, 33, 35, 36] overlapping and non-overlapping areas between range images need to be identified. The most accurate data is retained while inaccurate data is removed from the overlapping zone, before the remaining range data is $zipped$ [35] into a single surface. The detection of overlapping areas is crucial for the success of direct surface merging approaches. Wang and Oliveira [37] proposed a Moving Least Squares algorithm for automati-

cally identifying and filling holes in point clouds in regions associated with smooth surfaces. Zhou and Liu [41] used k-means clustering to improve the accuracy of detection of overlapping areas. Direct surface merging approaches can fill holes in the model with a patch that has the topology of a disc, but has difficulty in filling convoluted holes [3]. Volumetric approaches [1, 2, 3, 7, 8, 9, 21, 22, 25, 27, 28, 30] are capable constructing watertight, non-redundant, surfaces with complex geometries. Unfortunately, volumetric approaches are also sensitive to depth discontinuities that lead to surface reconstructions which are less plausible than those obtained by smoothly extending the observed surface data. While we do believe that model based approaches [24, 32] are capable of overcoming the depth discontinuity problem, the ability to formulate a model of the object to be reconstructed then becomes an unavoidable prerequisite.

Most of the integration approaches reported have been designed to operate on 3D data obtained from active 3-D scanners. Because of self occlusion, some parts of an imaged object surface are hidden and therefore a depth discontinuity appears in the corresponding range image. This depth discontinuity can be detected by calculating the angles between the local surface normals of the acquired object and the optical axis of the camera (or projector, in the case of active illumination systems), if the range signal to noise ratio is high enough. Local surface patches whose surface normal-optical axis angles exceed a certain threshold are treated as regions corresponding to depth discontinuities [26]. Alternative measures based on the same concept have also been reported [7, 8, 9, 35]. Because of the low level of noise in range data recovered by active scanners during surface measurement, the above approaches are usually adequate to label correctly all of the data corrupted by depth discontinuities. In the case of a stereo photogrammetry based 3D vision system, the problem of detecting depth discontinuities becomes more complicated. Firstly, in an area-based image matching system, the search process can incorrectly select correspondences biased toward depth discontinuities that produce high correlation scores, but unfortunately incorrect matches. Secondly, the noise level of the recovered range data is higher than that acquired by active scanners. Hence, the surface normals calculated from range images obtained via stereo photogrammetry are also correspondingly noisier. Such compromised range data will tend to cause classical volumetric integration approaches to fail. The practical consequence of failed integration is the corruption of merged object surfaces.

Here we propose a self-correction approach to constructing a watertight non-redundant surface from multi-view range images. Using a space carving algorithm [2], a watertight mesh is constructed from range images which have possibly been contaminated by depth discontinuities. Thereafter, non-contaminated range surface data is extracted from the range images and used to correct depth discontinuity induced damage to the integrated mesh by means of an elastic deformation. Details of our self-correction approach are presented in the section 4. We introduce our 3D photogrammetry stereo imaging system in section 2 and explain the discontinuity problem in section 3; and then present the detailed 3D shape reconstruction process using our self-correction approach in the section 4. Finally, examples of reconstructions based on our new approach are presented in section 5.

2. The 3-D Stereo Imaging System

In the work reported here we have adopted the C3D stereo imaging system to capture the 3D surfaces of humans and live animals [13, 14]. The system can be configured with multi-view stereo-pairs of high resolution cameras to meet the needs of a wide variety of applications. By adopting commercially available, professional-quality, high-resolution digital cameras, it is possible to obtain high-resolution colour images of 4000x4000 pixels (or greater) with current technology. In the 3D capture scenarios considered here, it is possible to acquire images that resolve local details of linear densities exceeding 0.1 mm/pixel. At such imaging resolutions there is enough local texture information on the object surface to achieve reliable area-based stereo matching [14, 38]. For example, we have configured two stereo-pairs of cameras (i.e. 4 cameras total) for human face measurement, three stereo-pairs for pig shape capture and four stereo-pairs for breast shape reconstruction. We define a camera stereo-pair to comprise a left and a right camera, and an image stereo-pair to comprise a left and a right image, each of these images being captured by the corresponding camera of the camera stereo-pair. The multi-view stereo pairs are configured to cover a specific region of interest from different view angles. The calibration facility within C3D requires that every camera, stereo-pair of cameras and stereo-pair combination captures views of a planar calibration target presented in varying poses within the imaged working volume. Standard bundles adjustment [29], initialized by means of the DLT (Direct Linear Transform) serves to recover the intrinsic and extrinsic parameters of each camera, thereby allowing the range maps acquired by each stereo-pair to be transformed into a common coordinate system. In operation, this calibration procedure achieves approximately 1pixel RMS re-projection error; and calibration is carried out before and after each capture session.

Following capture of multi-view stereo-pair images depicting the object, the C3D matching algorithm (based on normalized cross-correlation and multi-resolution search) is applied to each stereo-pair to compute horizontal and vertical image disparities. In addition, a confidence map is computed that reflects the local match correlation scores,

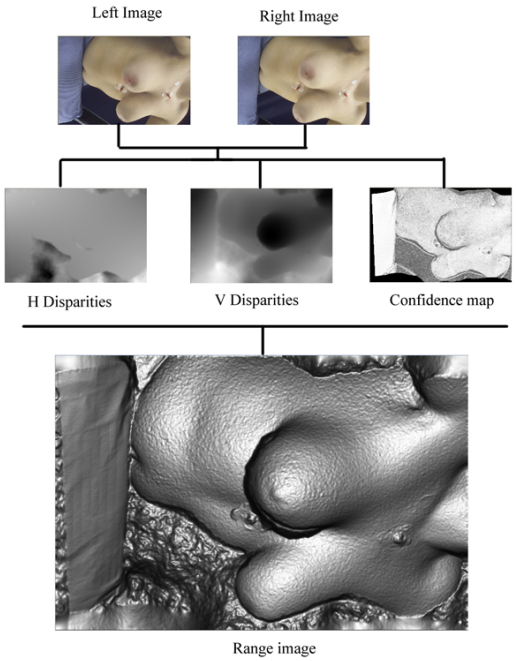

Figure 1. A stereo-pair of images acquired and processed

bounded to $[0.0, 1.0]$, at corresponding locations in the stereo-pair images (Figure 1). The value of each element in the confidence map is the correlation $c(i, j)$ between each local corresponding pixel centered patch $I_L(i, j)$ in the left image and $I_R(i - d_H, j - d_V)$ in the right image. Here, $d_H(i, j)$ and $d_V(i, j)$ are the horizontal and vertical disparities respectively:

$$c(i,j) = \arg\max_{d_H, d_V}(I_L(i,j) \circ I_R(i - d_H, j - d_V)) \quad (1)$$

Range images are calculated from the disparities by means of triangulation and the camera calibration parameters recovered by means of bundles adjustment [29]. In our system, range images are implicitly registered, since they are transformed into common world coordinates (X, Y, Z maps), defined by system calibration. A range image is defined in a generalized form:

$$r = r(i,j) \quad (2)$$

where (i, j) is the coordinate pair specifying the location of a range image element, r is the distance from the optical center of the left camera to the point $P(x, y, z)$ on the object surface. P is calculated from the disparities at (i, j). The next step is to integrate the range images into a watertight, non-redundant, surface model and our self-correction approach is then applied at this stage.

3. The Effects of the Depth Discontinuity

The range images are integrated into a watertight mesh via $spacecarving$ [2]. The resolution of the generated surface mesh can be adjusted by setting the size of the $marching\ cubes$ [19] employed in its reconstruction. Due to self-occlusion, there can be dent artifacts in the range images. As we can see in Figure 1, the surface at the left of the right breast is dented. More dents can be seen in Figure 4. Depth discontinuities have contaminated the range images to cause the integrated surface/mesh to dent (Figure 2, shadowed region). Our self-correction approach is able to repair such dents.

Suppose we have two range images A and B merged by the space carving algorithm: in this example the range image B contains contaminated data in the shadowed area in Figure 2 and the range image A also contains contaminated data in the grey area. The contaminated range data could lead to incorrect classifications of the voxels on the surface in the shadow region and grey regions shown in Figure 2).

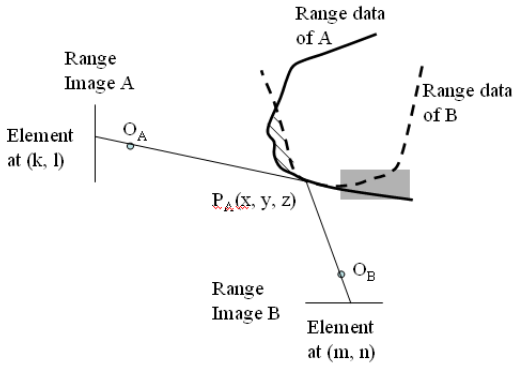

Figure 2. Illustration of artifacts produced by depth discontinuities

One option is to select the furtherest surface as the valid surface that will result in the range data B, in the shadow region, being selected which would be $wrong$ for the integrated surface. The integrated surface would be dented by the contaminated range data of B in the shadowed region. Another option is to select the nearest surface as the valid surface, such that the range data A in the shadowed region is selected. While this would be correct, this option could lead to the other parts of the surface being classified incorrectly, such as the grey region. Removing all depth discontinuity regions from range images, and then applying the space carving algorithm would leave holes and gaps in the integrated surface (Figure 8) if the surface to be captured could not be covered by all the range images. Hence, we devised our self-correction approach to overcome the problems caused by the depth discontinuities in the volumetric approach.

4. The Self-correction Approach

Our self-correction approach comprises three major steps:

- Integrating range images using the space carving algorithm: the results of this step can be seen in [2, 19], to obtain a watertight mesh. The resolution of the mesh can be adjusted by setting the size of the marching cubes [19].
- Processing confidence map to create masks: the masks are used to identify valid range data which represent the valid object surface.
- Iteratively deforming the integrated mesh towards the valid range data.

4.1. Create Masks from the Confidence Maps

Figure 3. Confidence maps generated by matching stereo-pairs of images

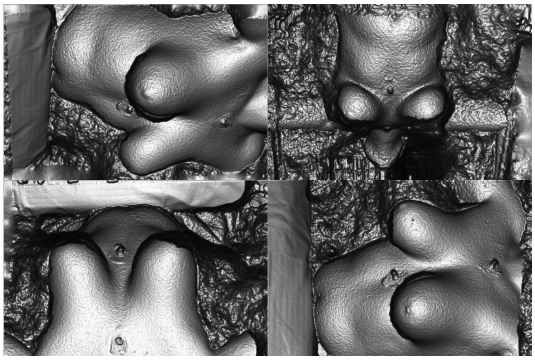

Figure 4. Range images calculated from recovered disparities

By observing the confidence maps (Figure 3) and range images (Figure 4) obtained though stereo matching, we were able to find relations between them. The bright regions in the confidence maps tended to correspond to valid object surfaces, and the other grey or dark regions in the confidence maps tended to correspond to either the discontinuities or non-object surfaces, i.e. the background. Based

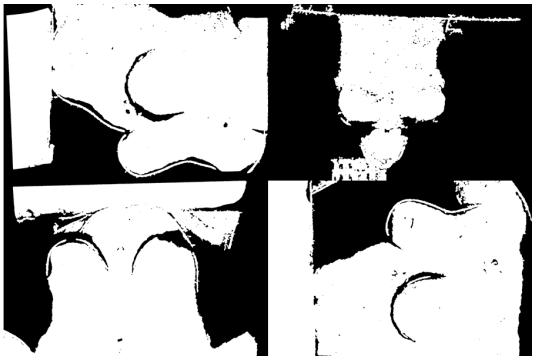

Figure 5. Masks labeling valid breast surfaces

on these observations, valid data selection masks (Figure 5) can be generated from the confidence maps by selecting the bright regions only. The confidence values are in the range [0.0, 1.0]. Each confidence map is converted to a grey level image with an intensity range [0, 255], prior to the $magic\ wand$ algorithm [20] being applied to provide a segmentation (tolerance parameter set to 60). We assume that the object always occupies the centre area of each image within each stereo-pair captured; this is ensured due to the configuration of our multi-view stereo system and by careful presentation of the object of interest to the system. Accordingly, the magic wand is initiated at the image centre. Narrow strips are observed along the edge of the object because of the application of area matching along the edges; where the confidence values are high but the correspondences are incorrect. We apply further morphological erosion and dilation [6] to remove the narrow stripes shown in Figure 5.

4.2. Self-repairing

In order to repair the dented surface $\bar{\boldsymbol{S}}$ of the integrated mesh, an elastic deformable model is applied to deform the $\bar{\boldsymbol{S}}$ into a plausible mesh $\boldsymbol{S}$ under the influence of valid range data r. The deformation of the integrated mesh is constrained by minimising the global energy of the mesh:

$$E(\boldsymbol{S}, \bar{\boldsymbol{S}}, r) = E_{ext}(\boldsymbol{S}, r) + \epsilon E_{int}(\boldsymbol{S}, \bar{\boldsymbol{S}}) \qquad (3)$$

where the parameter ϵ controls the trade-off between attractions of similar geometry and physical constraints. The external energy term E_{ext} attracts the vertices of the mesh to their most similar valid range data on the range images. It is defined as:

$$E_{ext}(\boldsymbol{S}, r) = \sum_{i=1}^{n} \omega_i k_{ie} \|\tilde{\boldsymbol{x}}_{\boldsymbol{i}} - \boldsymbol{x}_{\boldsymbol{i}}\|^2 \qquad (4)$$

where n is the number of vertices on the mesh; k_{ie} is an external spring constant; $\boldsymbol{x_i}$ is the ith vertex of $\boldsymbol{S}$; $\tilde{\boldsymbol{x}}_{\boldsymbol{i}}$ is its most similar valid point on the range images r; w_i is a weight related to the similarity between local surface

patches at $\boldsymbol{x_i}$ and $\tilde{\boldsymbol{x_i}}$. The internal energy term constrains the movement of the mesh and hence helps to maintain the original topology:

$$E_{int}(\boldsymbol{S}, \bar{\boldsymbol{S}}) = \sum_{i=1}^{n} \sum_{j=1\&j\neq i}^{n} k_{ij} \|(\boldsymbol{x_i} - \boldsymbol{x_j}) - (\bar{\boldsymbol{x_i}} - \bar{\boldsymbol{x_j}})\|^2 \tag{5}$$

where $\boldsymbol{x_i}$ and $\boldsymbol{x_j}$ are neighbouring vertices of $\boldsymbol{S}$; $\bar{\boldsymbol{x_i}}$ and $\bar{\boldsymbol{x_j}}$ are their original positions in $\bar{\boldsymbol{S}}$, k_{ij} is an internal spring constant. Since the energy function is quadratic with respect to $\boldsymbol{x_i}$, the optimization problem can be reduced to the solution of a sparse system of linear equations. This linear system can be efficiently solved using the conjugate gradient method. The positions of the vertices $\boldsymbol{x_i}$ are updated iteratively until the distances between $\boldsymbol{x_i}$ and $\tilde{\boldsymbol{x_i}}$ are less than a specified threshold.

Prior to local optimization deformation, each vertex in the mesh has to find its most plausible corresponding point on the range images. If the vertex finds its point, the vertex is labeled with TRUE; otherwise FALSE. The self-correction algorithm is embedded into the deformation process in the following steps:

1. Find the most plausible points on the range images for all vertices $\boldsymbol{x_i}$ of the mesh; label each vertex which has found its point with TRUE and calculate its displacement $(\tilde{\boldsymbol{x_i}} - \boldsymbol{x_i})$, otherwise label it with FALSE.

2. Update neighbouring points

   a. Get one vertex labeled with FALSE.

   b. Find the neighbours of the vertex.

   c. If all its neighbours are labelled with FALSE, go to "a" and get another vertex; otherwise translate the vertex with the mean displacement of the displacements of its neighbours labelled as TRUE; and also label it as TRUE.

   d. Repeat the steps "a" to "c" until no vertex is labelled with FALSE.

3. After all vertices have updated their positions, calculate their optimal positions by minimising the global energy of equation (3). Update the values of $\boldsymbol{x_i}$ for the next iteration.

4. Repeat the steps 2 to 4 until the differences between $\boldsymbol{x_i}$ and its most similar valid point on the range images $\tilde{\boldsymbol{x_i}}$ are less than a threshold.

5. Case Study Results

The self-correction approach has been tested on breast and pig shape reconstructions and both cases showed improvements in the quality of the integration of the range images.

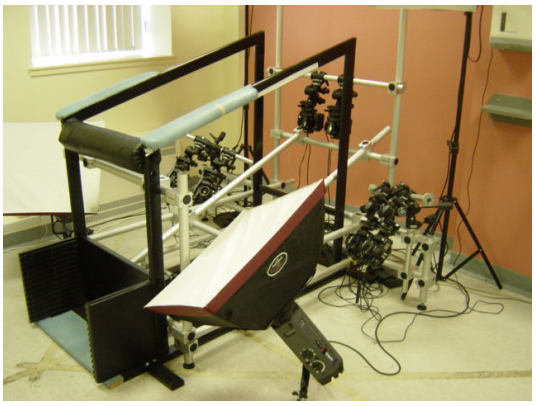

Figure 6. The breast capture rig comprising four stereo-pairs of cameras

Figure 7. Mesh representing the breast surface integrated from four range images

For breast shape reconstruction, four stereo-pairs of images were configured to cover the region of the breasts (Figure 6), where the camera stereo-pairs captured stereo-pair images from front, floor and left and right sides. The patients leaned over the rig in order to open the infra mammary fold and thereby exposed the entire area of each breast for image capture.

Four range images, with their corresponding confidence maps, were calculated and then integrated through the volumetric approach resulting in a single mesh of the breast (Figure 7).

According to heuristics embedded within the volumetric integration algorithms, the "best" range data from different

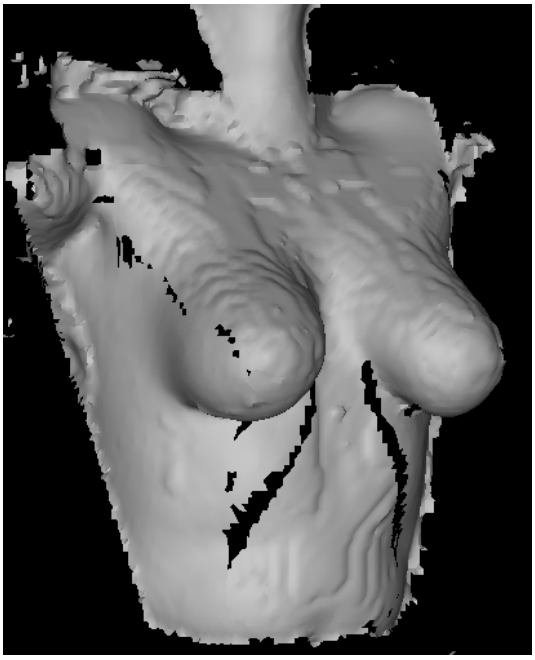

Figure 8. Mesh representing the breast surface integrated from four range images with masking

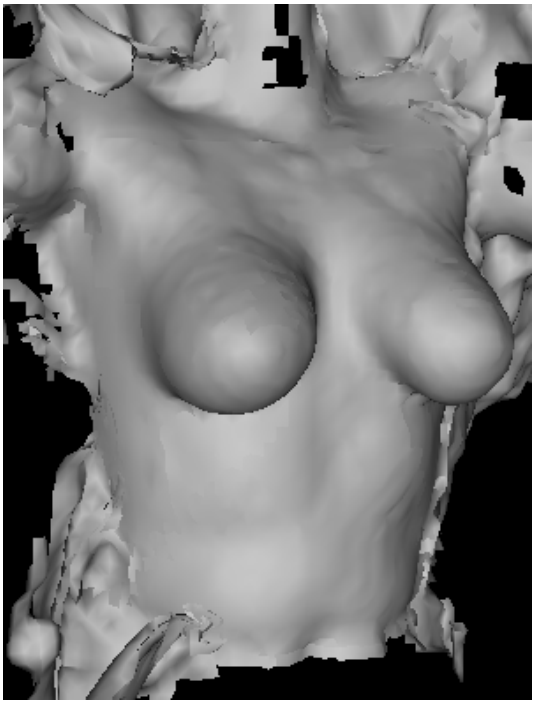

Figure 9. The corrected mesh representing the breast surface integrated from four range images with masks identifying plausible range data

views is selected to represent the surface of the breast. Unfortunately, if dented range data is selected to replace the valid surface, dents would appear in the model. Masks are calculated from the confidence maps by selecting the bright (i.e. confident) regions with the magic wand algorithm followed by morphological cleaning. The masks are used here to define in the range images valid range surfaces which are likely to represent the real shape of the breast captured. We attempted to apply the masks within the space carving algorithm to merge the range images as well. However, this approach produced integrated surfaces with gaps and holes (Figure 8). Of course, the gaps and holes could be filled by the other direct surface merging or volumetric integration algorithms, but here we propose an alternative approach which generates a watertight mesh by smoothly extending the observed surfaces. The volumetric approach has its limits and we have only been able achieve an improvement by applying our self-correction approach to the mesh obtained by the integration process (Figure 7) and by then deforming this mesh to the shape of the valid range data defined by the masks. We captured the shape of the breasts (Figure 9) by deforming the mesh elastically and iteratively. The dents in Figure 7 have been repaired; no gaps and holes in the region of the breast remain and the breast surface has been smoothed due to the elastic optimisation defined in equation (1). For this breast model, comprising 26887 triangular polygons, the optimisation process took approximately 20 seconds to compute using a P4 3.2GHz CPU with 4Gb of RAM. We believe that there is still room to improve the computational efficiency of the algorithm.

Figure 10. Mesh representing the pig generated from three range images

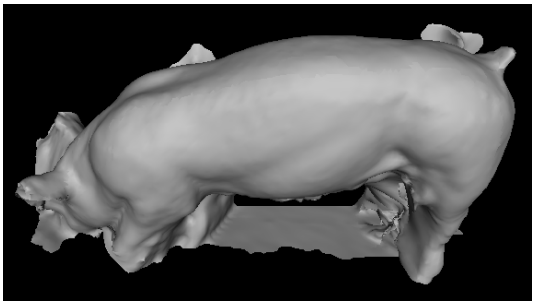

Figure 11. The corrected pig mesh with masks identifying plausible range data

The self-correction approach has also been applied to pig shape reconstruction. Three stereo-pairs of cameras were configured to cover the ham area of the pig from the side, top and rear views. The C3D stereo matching process was applied to recover three range images which were then merged into a single mesh (Figure 10). The resulting mesh of the pig had dents due to the shortcomings of the volumetric integration approach. After applying our self-correction approach to the mesh with masks, the dents in the mesh were corrected and a mesh that better represented the captured pig was produced (Figure 11). For this pig model, comprising 39779 triangular polygons, the optimisation process took apprximately 40 seconds to compute using a P4 3.2GHz CPU with 4Gb of RAM.

6. Conclusions

Our contribution here is the development of a novel range surface integration approach which is capable of repairing dent artifacts in meshes integrated from multi-view range images, which are evident in standard volumetric integration approaches. We first generate a watertight mesh from the range images; then generate masks from the confidence values produced by stereo matching to select viable range data; the final watertight mesh is obtained by deforming the mesh to the viable range data. Preliminary results demonstrate that our self-correction approach has the potential to reconstruct 3D shape from multi-view range images. We have succeeded in demonstrating the self-correction approach when applied to capturing the surface shape of complex objects such as breasts and live pigs. Our next task is to evaluate further the robustness, accuracy and reliability of this process.

References

[1] J. C. Carr, R. K. Beatson, J. B. Cherrie, T. J. Mitchell, W. R. Fright, B. C. McCallum, and T. R. Evans. Reconstruction and representation of 3d objects with radial basis functions. In *SIGGRAPH01*, pages 67–76, New York, NY, USA, 2001. ACM.

[2] B. Curless and M. Levoy. A volumetric method for building complex models from range images. In *SIGGRAPH*, pages 302–312, 1996.

[3] J. Davis, S. R. Marschner, M. Garr, and M. Levoy. Filling holes in complex surfaces using volumetric diffusion. In *Proc. First International Symposium on 3D Data Processing Visualization and Transmission*, pages 428–861, June 19–21, 2002.

[4] T. K. Dey, S. Goswami, and T. Cocone. A watertight surface reconstructor. *Journal of Computer and Information Science and Engineering*, 13:302–307, 2003.

[5] C. Dyer. Volumetric scene reconstruction from multiple views. In L. S. Davis, editor, *Fundations of Image Understanding*, chapter 16, pages 469–489. 2001.

[6] R. C. Gonzalez and R. E. Woods. *Digital image processing*. Prentice Hall, 2007.

[7] A. Hilton and J. Illingworth. Geometric fusion for a hand-held 3d sensor. *Machchine Vision and Applications*, 12:44–51, 2000.

[8] A. Hilton, A. J. Stoddart, J. Illingworth, and T. Windeatt. Reliable surface reconstruction from multiple range images. In *ECCV96, 4th European Conference on Computer Vision*, April 15-18 1996.

[9] A. Hilton, A. J. Stoddart, J. Illingworth, and T. Windeatt. Implicit surface-based geometric fusion. *Computer Vision and Image Understanding*, pages 273–291, March 1998.

[10] H. Hoppe, T. DeRose, and T. Duchamp. Surface reconstruction from unorganized points. *Computer Graphics*, 26(2):71–78, 1992.

[11] J. Isidoro and S. Sclaroff. Stochastic mesh-based multview reconstruction. Technical Report 2003-016, Boston University Computer Science Tech, July 2003.

[12] X. Ju, T. Boyling, J. P. Siebert, N. McFarlane, J. Wu, and R. Tillett. Integration of range images of multi-view stereo system. In *ICPR2004*, pages 280–283, 2004.

[13] X. Ju, T. Boyling, and P. Siebert. A high resolution stereo imaging system. *3D Modelling 2003*, 2003.

[14] X. Ju, P. Siebert, N. McFarlane, J. Wu, R. Tillett, and P. Schofield. A stereo imaging system for the metric 3d recovery of porcine surface anatomy. *Sensor Review*, 24(3):298–307, 2004.

[15] Y. Kawai, T. Ueshiba, T. Yoshimi, and M. Oshima. Reconstruction of 3-d objects by integration of multiple range data. In *ICPR92*, pages 154–157, 1992.

[16] K. Kolev and D. Cremers. Integration of multiview stereo and silhouettes via convex functionals on convex domains. *ECCV 2008, LNCS 5302*, pages 752–765, 2008.

[17] M. Lhuillier and L. Quan. Surface reconstruction by integrating 3-d and 2d data of multiple views. In *ICCV2003*, pages 1313–1320, 2003.

[18] X. Li and W. G. Wee. Range image fusion for object recognition and modelling. In *First Canadian Conference on Computer and Robot Vision*, pages 306–314, 2004.

[19] W. E. Lorensen and H. E. Cline. Marching cubes: A high resolution 3d surface construction algorithm. *ACM SIGGRAPH Computer Graphics*, 21(4):163–169, 1987.

[20] B. Marcotegui and F. Zanoguera. Image editing tools based on multi-scale segmentation. *ISMM2002*, pages 127–135, 2002.

[21] P. J. Narayanan and T. Kanade. Virtual worlds using computer vision. In *the 1998 IEEE and ATR Workshop on Computer Vision for Virtual Reality Based Human Communications*, pages 2–13, January 1998.

[22] S. Y. Park and M. Subbarao. Automatic 3d model reconstruction based on novel pose estimation and integration techniques. *Image and Vision Computing*, 22:623–635, 2004.

[23] R. Pito. Mesh integration based on co-measurements. In *IEEE Int. Conf on Image Proc.*, pages 397–400, 1996.

[24] R. Plankers and P. Fua. Articulated soft objects for multiview shape and motion capture. *PAMI*, 25(9):1182–1187, 2003.

[25] K. Pulli, T. Duchamp, H. Hoppe, J. McDonald, L. Shapiro, and W. Stuetzle. Robust meshes from multiple range maps. In *Int. Conf. On Recent Advances in 3-D Digital Imaging and Modelling*, May 1997.

[26] S. Rusinkiewicz, O. Hall-Holt, and M. Levoy. Real-time 3d model acquisition. In *SIGGRAPH 2002*, pages 438–446, 2002.

[27] M. Rutishauser, M. Stricker, and M. Trobina. Merging range images from arbitrarily shaped objects. In *IEEE Conference of Computer Vision and Pattern Recognition*, pages 573–580, 1994.

[28] R. Sagawa, K. Nishino, and K. Ikeuchi. Adaptively merging large-scale range data with reflectance properties. *PAMI*, 27:392–405, 2005.

[29] C. C. Slama, editor. *Manual of Photogrammetry*. American Society for Photogrammetry and Remote Sen, 5410 Grosvenor Lane, Suite 210, Bethesda, MD 20814-2160, USA., 1980.

[30] M. Sormann, C. Zach, J. Bauer, K. Karner, and H. Bishof. Watertight muli-view reconstruction based on volumetric graph cuts. In B. Ersboll and K. Pedersen, editors, *Proceedings of Scandinavian Conference on Image Analysis (SCIA 2007)*, volume 4522, pages 393–402, 2007.

[31] M. Soucy and D. Laurendeau. A general surface approach to the integration of a set of range views. *PAMI*, 17(4):344–358, 1995.

[32] J. Starck and A. Hilton. Model-based multiple view reconstruction of people. In *ICCV2003*, pages pp915–922, 2003.

[33] Y. Sun, J. Paik, A. Koschan, and M. Abidi. Surface modeling using multi-view range and color images. *Int. J. Comput. Aided Eng.*, 10(1):37–50, 2003.

[34] R. Tsai. A versatile camera calibration technique for high-accuracy 3d machine vision metrology using off-the-shelf tv cameras and lenses. *IEEE JOURNAL OF ROBOTICS AND AUTOMATION*, 3(4):323–344, Aug. 1987.

[35] G. Turk and M. Levoy. Zippered polygon meshes from range images. In *SIGGRAPH94*, July 24-29 1994.

[36] J. Wang and M. Oliveira. Improved scene reconstruction from range images. In *EUROGRAPHICS 2002*, volume 21, 2002.

[37] J. Wang and M. M. Oliveira. A hole-filling strategy for reconstruction of smooth surfaces in range images. *Computer Graphics and Image Processing, 2003. SIBGRAPI 2003. XVI Brazilian Symposium on 2003*, pages 11–18, 2003.

[38] J. Wu, R. Tillett, N. McFarlane, X. Ju, P. Siebert, and P. Schofield. Extracting the three-dimensional shape of live pigs using stereo photogrammetry. *Computers and Electronics in Agriculture*, 44:203–222, 2004.

[39] Z. Zhang. A flexible new technique for camera calibration. *IEEE Transactions on Pattern Analysis and Machine Intelligence*, 22(11):1330–1334, Nov. 2000.

[40] H. Zhou and Y. Liu. Incremental point-based integration of registered multiple range images. In *IECON 2005*, pages 468–473, 2005.

[41] H. Zhou and Y. Liu. Accurate integration of multi-view range images using k-means clustering. *Pattern Recognition*, 41:151–175, 2008.